A review of recent results on electrochemical determination of the density of electronic states of nanostructured metal-oxide semiconductors and organic hole conductors

Juan Bisquert [a,*], Francisco Fabregat-Santiago [a], Iván Mora-Seró [a],
Germà Garcia-Belmonte [a], Eva M. Barea [a], Emilio Palomares [b]

[a] *Department de Física, Universitat Jaume I, 12071 Castelló, Spain*
[b] *Institute of Chemical Research of Catalonia (ICIQ), Avda. Països Catalans 16, 43007 Tarragona, Spain*

Dedicated to Professor Michael Grätzel.

Abstract

The paper reviews recent results on electrochemical methods applied to the determination of the density of electronic states in several components of advanced nanostructured devices such as the dye solar cell (Grätzel cell), switchable displays, and sensors. We discuss the application of cyclic voltammetry and impedance spectroscopy to determine the chemical capacitance of mesoporous metal-oxide semiconductors (mainly TiO_2), organic hole transport materials, and molecular functionalizing elements.
© 2007 Elsevier B.V. All rights reserved.

Keywords: Dye solar cell; Nanostructured semiconductor; Organic conductor; Impedance spectroscopy; Cyclic voltammetry

1. Introduction

The work of Michael Grätzel has opened a new class of photoelectronic devices, those based on nanostructured metal-oxide semiconductors. These materials, and most prominently the archetypal TiO_2, are easy to process, are chemically and mechanically robust, and are efficient electron conductors. However, they are not generally photoactive unless they are in the UV spectral region. A nanostructured matrix of metal-oxide nanoparticles (or other nano-objects such as long rods) is well suited to host surface-attached organic components that extend the sensitivization to the visible spectrum, and also hole- or ion-conducting media that fill the nanopores. In this way, high and low energy levels in molecular components in the TiO_2 surface can be addressed with n-type and p-type

materials, respectively, from the external electrodes. This idea gave rise to the dye-sensitized solar cell (DSC) [1–3], generally known as the Grätzel cell, that constitutes a milestone in the search for cheap and efficient photovoltaic devices. Functionalization of metal-oxide nanostructures is rather versatile, and has given rise to other applications, many of them pioneered by Grätzel and his coworkers as well, such as the photoelectrochromic device obtained by anchoring viologen molecules in the surface of TiO_2 [4]; biological sensors [5]; and ambipolar devices formed by switchable electron/hole conduction along an organic monolayer in the metal-oxide surface [6].

Crucial to the development of these types of devices is a sound understanding of the energetics of electronic carriers in the metal oxide, in the organic hole conductors, and in the molecular functionalizing elements in the metal-oxide surface. Such energetics influences a number of electronic phenomena, i.e. how many carriers are stored in each of the phases of the device when a voltage difference (related

---
* Corresponding author.
E-mail address: bisquert@uji.es (J. Bisquert).

to carriers Fermi levels displacement) is established at the contacts? And what is the rate of electronic transitions between neighboring phases inside the device? A key piece of information for answering such questions in specific situations, is the density of states (DOS) in the different phases constituting the particular device.

In recent years, it has been recognized that standard electrochemical techniques such as cyclic voltammetry (CV) and impedance spectroscopy (IS), under a certain set of broad conditions, constitute effective methods of determining the DOS in metal-oxide nanostructured semiconductors [7,8] and also in organic conductors [9,10]. Such techniques have been used to a large extent in order to investigate the properties of nanostructured devices based on the metal-oxides with different types of surface functionalization [11–18]. This paper provides a short summary of these methods, emphasizing both the physical principles lying behind the experimental methods and the applications in various kinds of devices. The paper describes the electrochemical determination of DOS in different materials that form part of nanostructured devices: the mesoporous metal-oxide semiconductors (usually electron conductors), quantum dots that exhibit size quantization effects, organic hole transport materials used in solid DSCs, and molecular functionalizing elements.

2. Chemical capacitance and density of states

2.1. Nanostructured semiconductors

Colloidal metal-oxide nanocrystals are usually deposited over a conducting substrate and are thermally treated to form a connected array of nanoparticles that can be used as electroactive electrodes. These structures normally form a random nanoparticulate network (RNN) with huge internal area. The degree of ordering can be increased [19], and there is a great deal of interest in metal-oxide nanotubes and nanorods vertically aligned on the conducting substrate [20–22]. However, the electrochemical properties of these regular structures have been less studied and our attention will be predominantly focused on RNN. Since the general theory for CV [7] has not been substantially modified, only a brief outline is presented here, and the extensions of the model [23] will be commented in due course.

When a voltage variation dV is applied to the conductive substrate of the nanostructured film, the Fermi level is displaced homogeneously as $dE_{Fn} = -q dV$ (where q is the elementary charge). Consequently the electron density changes by a quantity dn. The electrochemical capacitance (per unit volume) [14,24] relates the change of number density of electrons, n, to the change of electrochemical potential

$$C_\mu = q \frac{dn}{dE_{Fn}} \qquad (1)$$

There are two basic mechanisms of accumulating charge with respect to voltage in electrochemical systems. The first one is a standard dielectric capacitor where energy is stored in the electrical field, related to spatial charge separation. This capacitance is ubiquitous at interfaces with space charge such as Schottky barriers and Helmholtz layers. In general, the dielectric capacitance is associated to charging the spatially separated plates of the capacitor with a displacement current. The second one consists on increasing the chemical potential of the species in a bulk material by increasing their number. Here the "plate" of the capacitor is charged by conduction current. This second case can be called the chemical capacitor [14,24] and it is specially relevant for ion intercalation materials, nanostructured semiconductors [14] and organic conductors [9].

Consider one specific electronic state characterized by the energy E. This energy is defined to be increasingly negative for states deeper in the gap. The average occupancy is described by the Fermi–Dirac distribution function

$$f(E - E_{Fn}) = \frac{1}{1 + \exp[(E - E_{Fn})/k_B T]} \qquad (2)$$

where k_B is Boltzmann's constant. A displacement of the Fermi level causes a variation of the state occupancy in the following way:

$$\frac{df}{dE_{Fn}} = \frac{1}{k_B T} f(1 - f) \qquad (3)$$

Assuming that the conduction band potential is stationary, when the voltage at the substrate is modified negatively, the Fermi level inside the TiO$_2$ nanostructure is displaced towards the conduction band. In this case, the change of electrochemical potential implies a change of the chemical potential of electrons, i.e. $dE_{Fn} = d\mu_n$. Eq. (1) gives a purely chemical capacitance [8]. For a single electronic state of density N, we therefore obtain
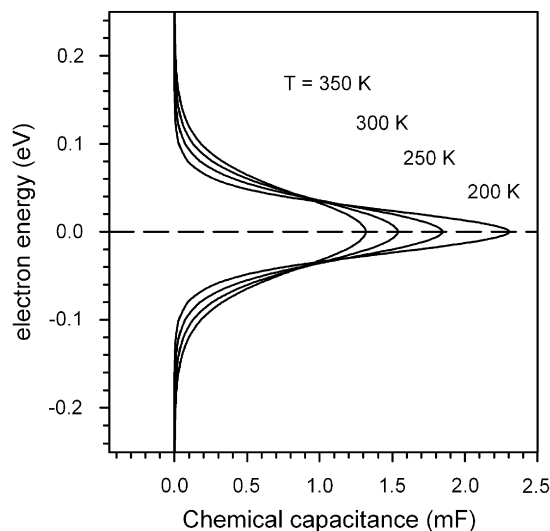

Fig. 1. Representation of the chemical capacitance of a monoenergetic energy level (dashed line) as a function of the temperature as indicated.

$$C_\mu = \frac{Nq^2}{k_B T} f(1-f) \qquad (4)$$

As indicated in Fig. 1, the chemical capacitance of a single state shows a thermal spread of 0.1–0.2 eV that increases with the temperature.

Consider now a distribution of states, $g(E)$, the DOS in the bandgap, as indicated in Fig. 2a. The chemical capacitance is obtained integrating all the contributions of available states

$$C_\mu(E_{Fn}) = q^2 \int_{-\infty}^{+\infty} g(E) \frac{df}{dE_{Fn}} dE$$
$$= \frac{q^2}{k_B T} \int_{-\infty}^{+\infty} g(E) f(E - E_{Fn})[1 - f(E - E_{Fn})] dE \qquad (5)$$

Assuming that Fermi–Dirac is a step function (i.e., the zero-temperature approximation), the function $f(1 - f)$ gives a Dirac-δ, and then Eq. (5) takes the form [23]

$$C_\mu(E_{Fn}) = q^2 g(E_{Fn}). \qquad (6)$$

It is therefore found that the chemical capacitance is proportional to the DOS. The interpretation of Eq. (6) is that the extent of charging related to the perturbation dV corresponds to filling a slice of traps at the Fermi level, and this is suggested in Fig. 2a.

A common finding in nanostructured TiO$_2$ is an exponential distribution of localized states in the bandgap as described by the expression

$$g(E) = \frac{N_L}{k_B T_0} \exp[(E - E_c)/k_B T_0]. \qquad (7)$$

Here N_L is the total density and T_0 is a parameter with temperature units that determines the depth of the distribution, which can be alternatively expressed in energy units $\varepsilon_0 = k_B T_0$ or as a coefficient $\alpha = T/T_0$. According to Eqs. (6) and (7) the chemical capacitance should display an exponential dependence on applied potential, and this is found experimentally as discussed in the next section. In addition, nanostructured TiO$_2$ usually shows a nearly monoenergetic state below the bandgap, which is suggested as a surface state in Fig. 2a. Therefore, the total chemical capacitance, due to occupation of electronic levels, is predicted to have the shape shown in Fig. 3.

2.2. Quantum dots

Quantum dots (QD) are nanocrystals of size roughly between 1 and 10 nm. The strong quantum confinement implies that insulating nanocrystals have a set of discrete atom-like valence and conduction energy levels. Their separation as well as the optical gap between the lowest conduction level and the highest valence level increases as the nanocrystal size decreases. Nanocrystals with a narrow size dispersion can be assembled into two-dimensional or three dimensional ordered arrays, which are termed nanocrystal superlattices. QDs are good candidates for sensitizers in DSCs [25–28]. The discovery of quantum efficiency higher than 100% by carrier multiplication in QDs [29–31], reaching even 7 excitons per absorbed high energy photon in PbSe colloidal nanocrystals [31], has stimulated renewed interest in this subject.

While photoexcitation creates electron–hole pairs, assemblies of quantum dots deposited on a conducting
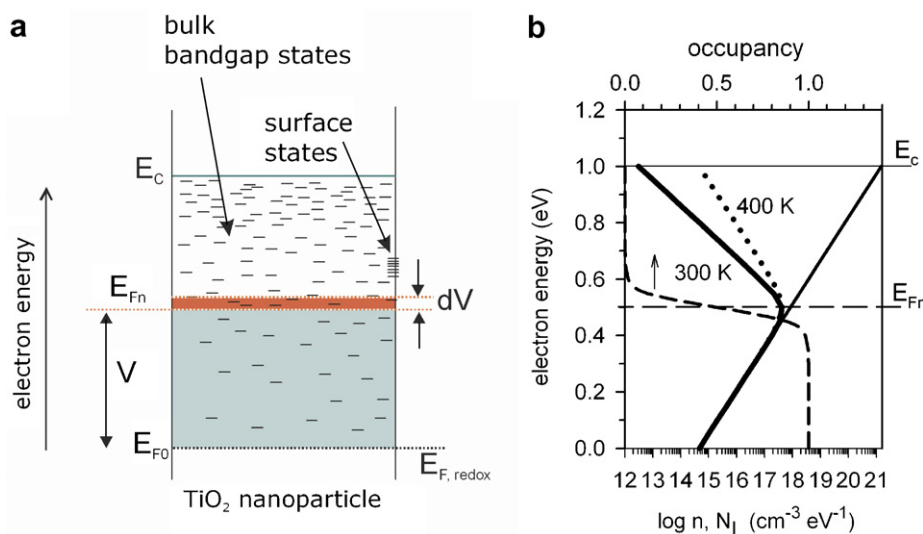

Fig. 2. (a) Schematic energy diagram of electronic processes governing electron transport in a TiO$_2$ nanoparticle in a DSC. E_{F0} shows the position of the Fermi level in the dark, which is equilibrated with the redox potential ($E_{F,redox}$) redox couple. E_{Fn} is the Fermi level of electrons accumulated in the nanoparticles and E_C is the conduction band energy. The shaded region indicates the bandgap states that are occupied with electrons below the Fermi level (zero-temperature approximation of Fermi–Dirac distribution). The square shows the filling of states under a small displacement of the Fermi level, under a potential step dV. (b) Quantitative representation of the thermal occupation at temperature $T = 300$ K (thick line) of an exponential DOS in the bandgap (thin line) with $T_0 = 800$ K and $N_L = 10^{20}$ cm^{-3}, as determined by the Fermi–Dirac distribution function (dashed line). The dotted line indicates the distribution of carriers at $T = 400$ K.

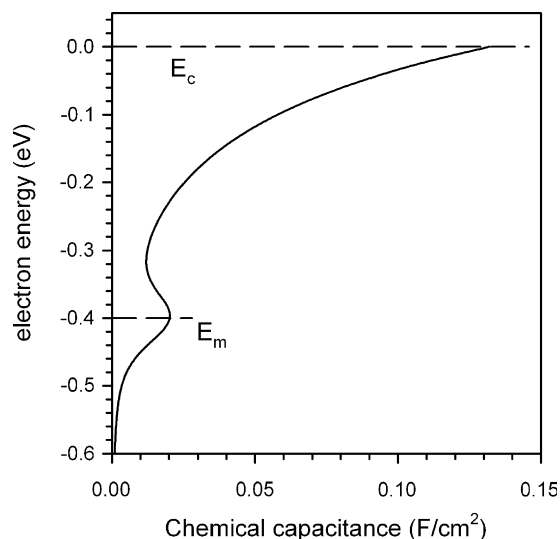Fig. 3. Representation of the chemical capacitance of an exponential distribution of states with density $N_{exp} = 10^{20}$ cm^{-3} below the lower edge of the conduction band ($E_c = 0$ eV) and a monoenergetic energy level with density $N_m = 10^{18}$ cm^{-3} ($E_m = -0.4$ eV) at temperature $T = 300$ K. Electrode of 10 μm thickness.

substrate, and filled with an ionic medium, allow the injection of a single kind of carrier in the superlattice, which permits to investigate the DOS electrochemically. The electrochemical potential of electrons injected in a superlattice depends on individual electronic levels for a quantum dot and also on Coulomb interactions, both for multiple electrons in a quantum dot and in neighbour dots [32]. Characteristic capacitance spectra showing consecutive charging of different discrete energy levels have been reported for assemblies of CdSe [33,34] and for arrays of monodisperse ZnO quantum dots [35,36]. The influence of size dispersion over collective transport properties in these systems has been examined theoretically [37].

2.3. Molecular species in solution

Since the Nernst formula is identical with Fermi–Dirac statistics, Eq. (4) and Fig. 1 also describe the chemical capacitance of a redox species, either in solution or when attached to the semiconductor surface. Such specific instance of a chemical capacitance was conventionally denominated "pseudocapacitance" [38] and sometimes "redox capacitance" [39].

The Marcus–Gerisher model [40,41] often provides a good description of charge-transfer between semiconductor and acceptor molecules in solution, and the model has been applied in DSCs [42,43]. Due to the thermal fluctuation and changes of polarization, the acceptor levels take the form of an effective Gaussian density of states, with a width given by the reorganization energy. However, this is not a real DOS in equilibrium, but a probability of charge-transfer [44]; therefore, this Gaussian distribution cannot be obtained as a chemical capacitance by CV or related

techniques. Instead, the effective Gaussian DOS can be obtained from the voltage-dependence of the heterogeneous rate constant [45].

On another hand, it is likely that molecular species adsorbed at the semiconductor surface display a degree of energetic disorder, and a Gaussian distribution is a good candidate to describe the DOS of the molecular levels in the presence of a disorder [46] as it is usually found in solid organic conductors.

2.4. Organic conductors

Organic hole conductors such as spiro-OMeTAD (chemical name 2,2′7,7′-tetrakis(N,N-di-p-methoxyphenylamine)-9,9′-spiro-bifluorene) constitute a key element to form nanostructured devices [47–49]. In organic conductors, disorder or structural correlations with correlation lengths of a few intermolecular distances (fluctuation in the local conjugation length) lead to a dispersion of energies. The most successful model for describing transport in organic conductor is a Gaussian disorder model developed by Bässler [50] using a regular array of hopping sites with a Gaussian distribution of site energies

$$g(E) = \frac{1}{\sqrt{2\pi}\sigma} \exp\left[-\frac{(E_0 - E)^2}{2\sigma^2}\right] \tag{8}$$

where E_0 is the center of the distribution and σ is the width. It is widely agreed that the distribution of electronic states in disordered organic conductors has a Gaussian shape, as recently observed by capacitance measurements [10,9,51,52]. The Gaussian distribution in organic semiconductors is caused by the fluctuation of the lattice polarization energies [50], dipole interactions [53] and molecular geometry fluctuations [54].

Considering a Gaussian distribution of holes states, the distribution is fully occupied above the Fermi level, and shows the thermal spread at the Fermi level, as depicted in Fig. 4. It can be shown [55,56] that if the density of holes is very low, the distribution of holes is given to a good
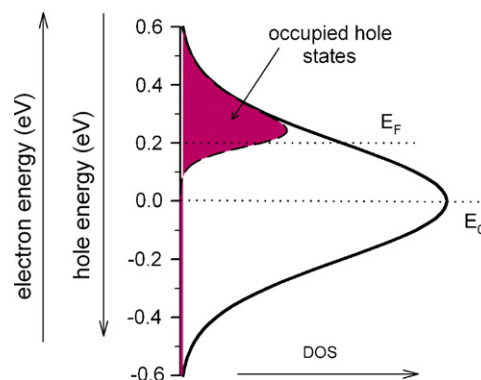

Fig. 4. Representation of a Gaussian DOS (center of the DOS $E_0 = 0$ eV, and width parameter $\sigma = 0.2$ eV). The shaded area shows the occupancy of the DOS with holes when the Fermi level is at 0.2 eV at $T = 300$ K.

approximation by a Gaussian centered at σ_P^2/k_BT above the mean of the DOS, independently of the position of Fermi level. However, this "Boltzmann regime" is obtained only when the Fermi level is higher than σ_P^2/k_BT above the mean of the DOS.

Most of our discussions have been so far based on the Fermi–Dirac (or Nernst) statistics. We should remark that this applies in the case of independent species randomly occupying the available sites. More generally, in the presence of interactions, the chemical capacitance relates to the electrochemical potential function on the number of carriers. For example, in amorphous intercalation materials, in particular in Li_xWO_3, the chemical capacitance mainly shows the contributions of the chemical potential of Li^+ inside the amorphous film, which is governed by elastic distortions of the host material [57–59].

3. Experimental techniques

The electrochemical methods for determination of the DOS in the mesoporous semiconductors (organic films) are based on the measurement of the variation of the density of electrons (holes) caused by a modification of Fermi level [14]; such variation relates to the chemical capacitance [8], as discussed above. Experimental methods include CV [7], impedance spectroscopy [60], voltage-decay charge-extraction [61–65] and potential step-current integration (chronoamperometry) [66,67].

The standard cyclic voltammetry technique [7] monitors the current injected in the film as the potential varies at a constant speed, $s = dV/dt$. The current density on a film of thickness L and porosity p is

$$j = -qL(1-p)\frac{dn}{dt} = q^2L(1-p)\frac{dn}{dE_{Fn}}\frac{dV}{dt} = L(1-p)sC_\mu \tag{9}$$

Hence, $C_\mu(E_{Fn})$ is measured directly by cyclic voltammetry. Fig. 5c illustrates that the shape of a CV directly reveals the shape of the DOS, using the case of an exponential distribution as an example.

Eq. (9) assumes that the voltage applied in the substrate of a nanostructured film is exclusively invested in displacing the Fermi level across the energy scale in the semiconductor. It requires that the voltage scan is slow enough for the film to reach equilibrium at each state of charging. The main experimental criterion for this is that the capacitive CV is symmetric with respect to the energy/voltage axis, corresponding to the fact that electrochemical capacitance may depend on potential but is independent of the sense of the current. Additional elements in the electrochemical cell, such as IR drops, and faradaic charge-transfer resistance at the metal-oxide/electrolyte interface, produce a distortion of the symmetric shape [7].

It should be remarked that Eq. (6) is an approximation for a continuous DOS that neglects the thermal spread affecting each state in the distribution. In reality the
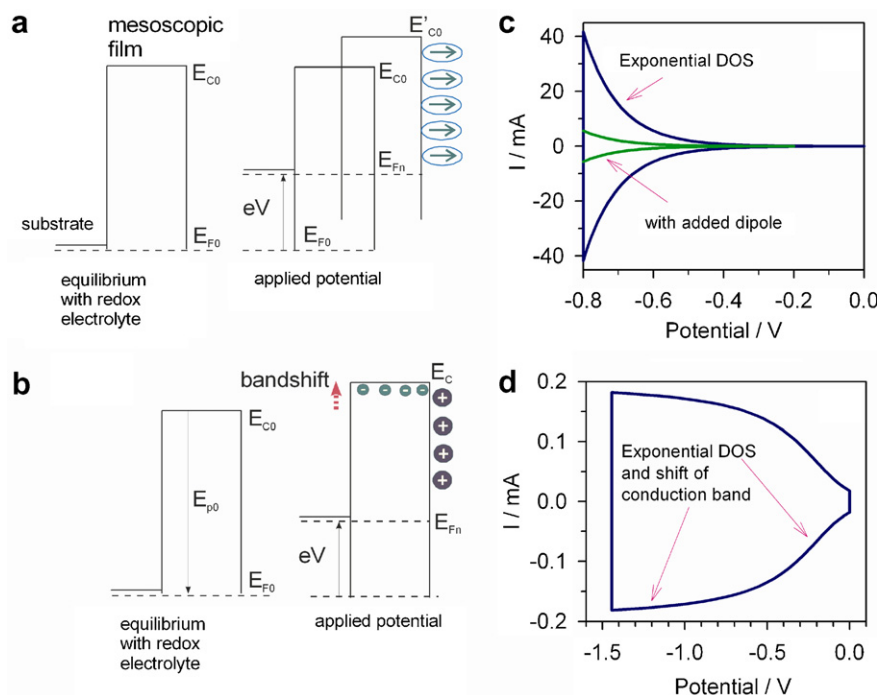

Fig. 5. The left column shows the schematic energy diagram of a nanostructured semiconductor under application of a potential that homogeneously rises the Fermi level in the film. (a) Stationary energy levels, and another case is shown in which modification of the semiconductor surface with dipolar molecules induces a permanent shift of the energy levels. (b) Shift of the energy levels along the increase of the electron density by modification of the Helmhotz potential at the nanoparticles surface by ionic compensating charge. The right column shows the corresponding CVs for an exponential distribution of bandgap states in the nanoparticles.

Fermi–Dirac function is not abrupt at E_{Fn}, as it is indicated in Fig. 2b. The exact relation consists on a convolution of the DOS over a function of the Fermi–Dirac function, Eq. (5). A procedure for obtaining the DOS from the measured C_μ by successive approximations has been developed [23,68]. This method provides highly accurate results by using only 4 orders of approximation at practical temperatures.

One important parameter for nanostructured devices is the position of the semiconductor conduction band/transport level. Such position can be readily modified by absorption of dipolar species at the metal oxide/electrolyte interface, as indicated in Fig. 5a. CV immediately reveals the global displacement of the semiconductor energy levels as a shift of the voltammetry along the potential axis, as illustrated in Fig. 5c.

For maintaining charge neutrality into a nanostructured film under electron accumulation, it is required that the increasing electron charge in the nanoparticles be accompanied by positive ion charge at the semiconductor/electrolyte interface. As shown in Fig. 5b, surface charging at increasing electron density in the nanoparticulate network changes the potential difference in the Helmholtz layer, producing an upward shift of the semiconductor energy levels [69]. The combined effect of electron accumulation and partial band unpinning can be accounted for by a constant Helmholtz capacitance, C_H, connected in series to the chemical capacitance, C_μ, so that the total electrochemical capacitance becomes

$$C = (C_\mu^{-1} + C_H^{-1})^{-1} \tag{10}$$

Hence when the exponentially increasing C_μ becomes larger than C_H, the CV flattens to a constant value, Fig. 5d, in consonance with the fact that the band shifts simultaneously with the displacement of the Fermi level, with a smaller rate of gain of electron density in the nanostructure.

IS is a voltage/current small perturbation frequency modulation method widely applied in DSC [70–77]. While CV is a fast large perturbation method that rapidly gives information about the whole DOS, IS requires a separate measurement at each steady state. However, the application of equivalent circuit analysis to the frequency domain data in IS is capable to provide the chemical capacitance in the presence of additional processes such as series and charge transfer resistance. Therefore, when faradaic currents are blocked, the voltammetries, Fig. 6a, may inform about the density of states in TiO$_2$ as its capacitance, Fig. 6b, may then dominate the current in a certain potential window. But on the other hand, in DSC the capacitive currents are hidden by much larger recombination current, as shown in Fig. 7a. In these cases, to observe the DOS it becomes necessary to measure the capacitance via IS as shown in Fig. 7b.

The electronic conductivity in nanostructured TiO$_2$ permeated with electrolyte solution can be measured by IS [73] and also directly in electrochemical transistor configuration shown in Fig. 8a [67,78]. Several studies have shown that the electronic conductivity is dependant on the density of electrons in the transport state (conduction band) [73,78,79]. Therefore, the conductivity can be used as an effective tool to monitor the displacement of the energy levels in the nanostructured semiconductor. As shown in Fig. 8b, molecular species absorbed in the TiO$_2$ surface [80] with different dipole moments cause a shift of the bands which is observed as the displacement of the conductivity plot along the voltage axis, as depicted in Fig. 5a.
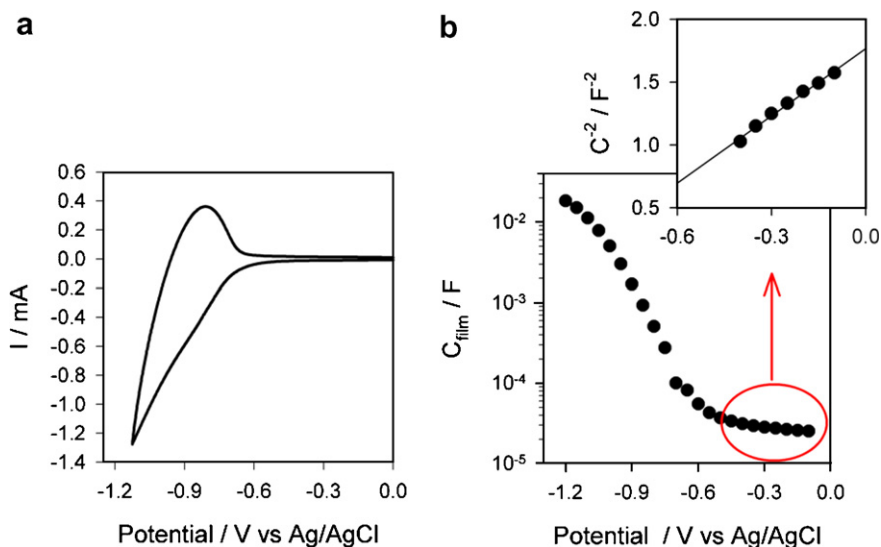

Fig. 6. Characteristic CV (a) and capacitance from IS (b) of a nanostructured TiO$_2$ film in a blocking electrolyte. At the more positive potentials the capacitance is dominated by Helmholtz layer at the uncovered transparent conducting oxide, as shown by the Mott–Schottky plot representation in the inset.
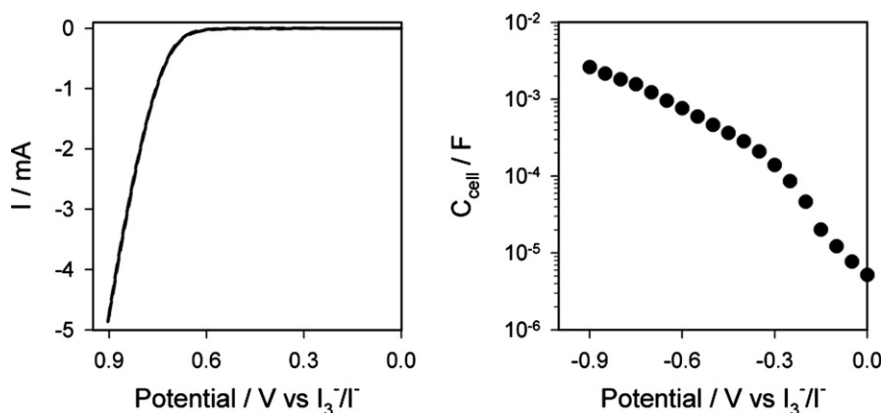
Fig. 7. (a) Voltammetry of a DSC in the dark current is dominated by recombination. (b) Capacitance of the TiO_2 in the cell obtained by IS.
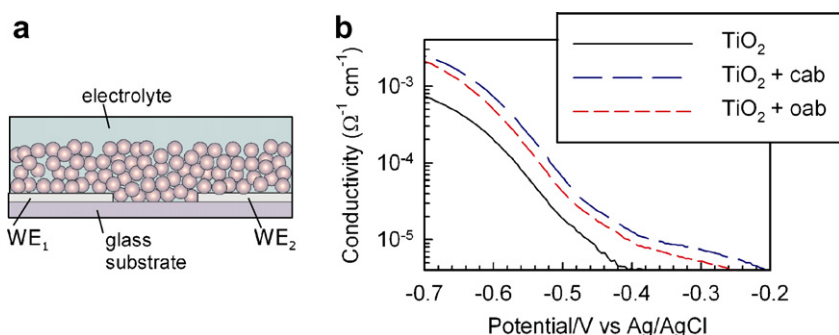

Fig. 8. (a) Electrochemical transistor measurement configuration. The conducting substrate over which the mesoporous film is deposited is divided two regions, working electrodes (WE) separated by an insulating gap. (b) Conductivity plot of a bare, mesoporous TiO_2 film and molecular modified films with electrochemically deposited 4-methoxybenzenediazonium tetrafluoroborate (oab) and 4-cyanobenzenediazonium tetrafluoroborate (cab). Reprinted with permission from [80]. Copyright (2005) The American Chemical Society.

4. Results on nanostructured metal-oxide films

4.1. General characteristics of the capacitance

The capacitive response of nanostructured TiO_2 films, and similarly in other undoped metal-oxide RNN, shows several characteristic features.

(a) The dominant feature is an exponential DOS at the negative potentials approaching the conduction band potential.
(b) In many cases, a symmetric and much less intense peak appears at less negative potentials, Fig. 9. In CV, these features are highly symmetric with respect to voltage axis in good quality electrodes, though they sometimes appear as a distortion due to IR drop. The symmetric shape of CV with the exponential increase and the additional peak at a more positive potential, that is theoretically depicted in Fig. 3, is very well established experimentally and appears in a large number of reports, since the first one in 1995 by Grätzel and co-workers [11]. A more recent report is shown in Fig. 9. Fig. 10 shows an even more
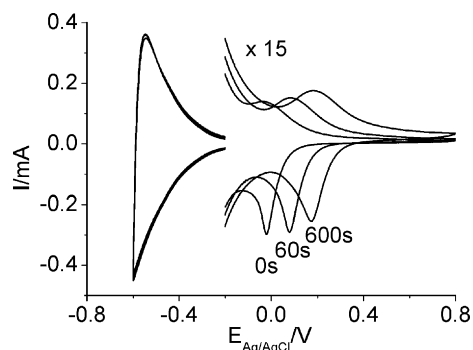

Fig. 9. Cyclic voltammograms of PI-KEM nanostructured TiO_2 electrode (50% anatase + 50% rutile, surface area 27 m^2 g^{-1}, thickness 8 μm, scan rate 20 mV s^{-1}, working solution 0.1 M HCl_4 purged with N_2) as a function of electroreduction time at −0.6 V. Reprinted from [82], with permission from Elsevier.

accurate resolution of the exponential DOS from CV by using the deconvolution procedure that was discussed above [68].

The capacitance shows additional features:

(c) At positive potentials a nearly constant capacitance is found, corresponding to the exposed surface of the conducting substrate. This capacitance is related to
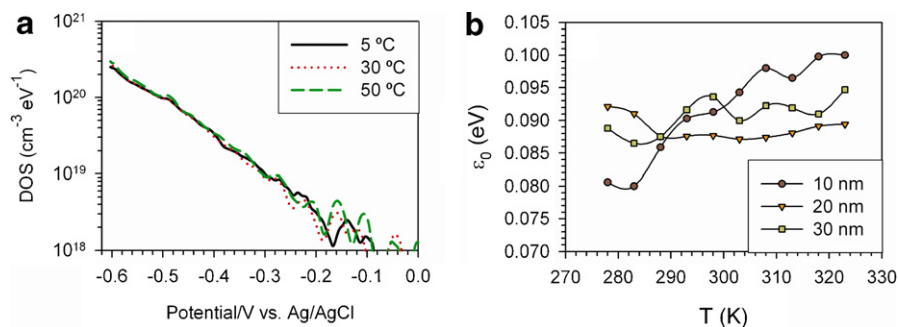
Fig. 10. (a) Fourth order approximation of the density of states obtained from CV at finite temperatures in nanostructured TiO_2 films of 20 nm radius as indicated. (b) Energy parameter $\varepsilon_0 = k_B T_0$ for an exponential DOS, resulting from a fit of the 4th order approximation of the DOS, to the distribution $g(E) = A \exp(E/\varepsilon_0)$, as a function of temperature in nanostructured TiO_2 films of different particle radii as indicated. Adapted from Ref. [68].
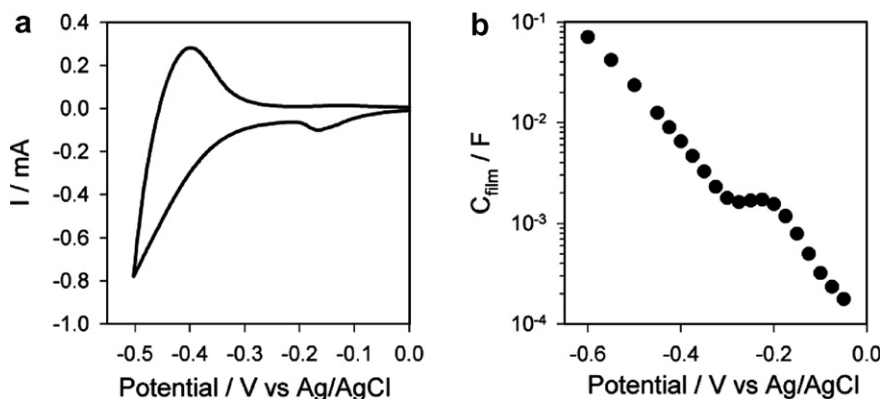

Fig. 11. (a) CV of TiO_2 film in aqueous solution at pH 2 presenting a surface state peak (b) capacitance of the same sample. The exponential growth of the capacitance is modified by the presence of the surface state.

depletion of the highly doped substrate and exhibits Mott–Schottky characteristics [81], see Fig. 6b.

(d) At very negative potentials, close to the conduction band edge, the capacitance is partially controlled by Helmholtz capacitance at the inner surface, and the film enters into band unpinning, Fig. 6b.

The origin of the exponential DOS in nanostructured TiO_2 is not conclusively established. Some studies of electron transport and recombination suggest that transport-limiting traps are located predominately on the surfaces of the particles [83]. A recent study of CV [68] found that for RNNs with particle sizes of 20 and 30 nm, the exponential distribution is nearly temperature-independent, which is the standard behaviour of band tailing in bulk semiconductors, either impurity-induced or as a consequence of local coulombic interactions and dislocations of the bulk lattice [84]. In contrast to this, for small (10 nm) nanoparticles, a temperature variation of width of the exponential distribution is found, Fig. 10b. Similar
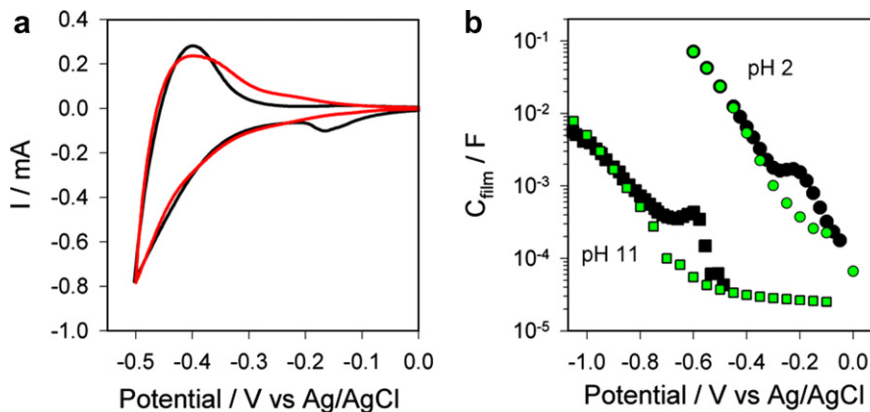

Fig. 12. The peak at low potentials disappears after aging the sample in several voltammetric and impedance measurements. (a) The effect for a TiO_2 film in aqueous solution at pH 2. (b) Effects on the capacitance at pH 2 (circles) and pH 11 (squares). Black before aging, green after aging.

observations have resulted from anomalous diffusion measurements by surface photovoltage (SPV) transients [85,86]. These observations have been interpreted by treating the TiO$_2$ nanoparticles as quantum dots, in terms of the confinement effect due to dielectric mismatch at the
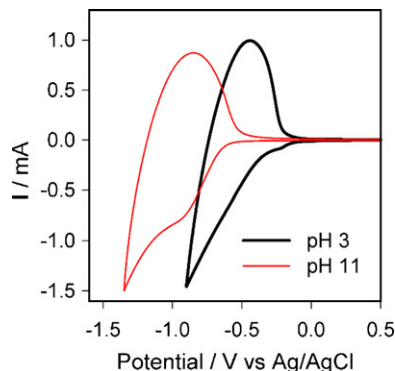

Fig. 13. CVs of TiO$_2$ sample at pH 11 and pH 3.

boundary between the quantum dot and the surrounding medium [68,87].

The peaks at the more positive potentials are observed in TiO$_2$ RNNs by both CV and IS, Fig. 11. These peaks are characteristic for nanostructured films and have not been obtained in polycrystalline electrodes [88]. The peaks have been interpreted as the reversible filling of surface states below the conduction band edge [11,89,90]. It has been noted that the surface state evolves with time, Fig. 9. In some cases, the peak may even disappear after aging by multiple cycling of the sample, Fig. 12. In other samples degradation takes place and the peak becomes more important.

4.2. Shift of conduction band

As is well known, changes in pH of the solution displace the conduction band of TiO$_2$ upwards or downwards according to the expression: $E_{cb} = E_{cb_0} - 59$ pH (at $T = 300$ K). In consequence, the CV is shifted in the
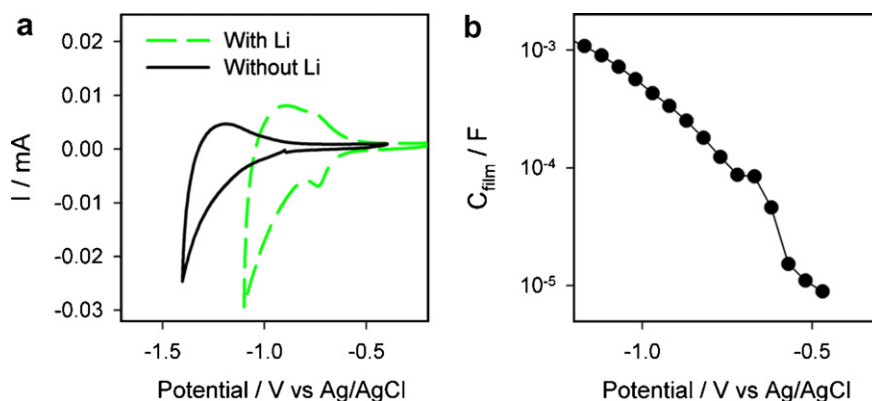

Fig. 14. (a) Cyclic voltammetries of a TiO$_2$ film in a room temperature ionic liquid (1-ethyl-3-methylimidazolium bis((trifluoromethyl)sulfonyl)amide, EMITFSI) with and without 0.1 M LiTFSI solution. In this case, the peak attributed to intraband Ti^{3+} surface states is only observed for the Li containing solution and rises with cycling. (b) Capacitance data for sample within the electrolyte containing Li ion. Reprinted with permission from [14]. Copyright (2006) The Royal Society of Chemistry.
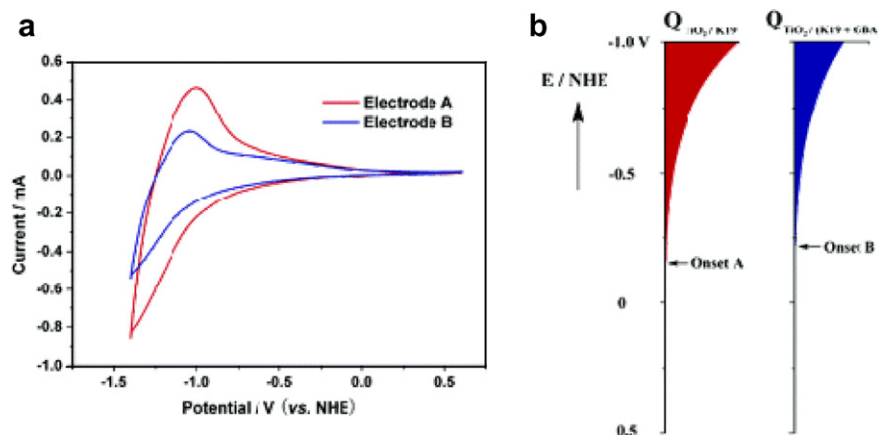

Fig. 15. (a) Cyclic voltametries of TiO$_2$ electrode A (K-19 grafted only) and electrode B (GBA cografted) in EMITFSI. Straight red line for Electrode A, coated with K-19 sensitizer alone; blue line for Electrode B, K-19/GBA cografted. The scan rate is 0.05 V s^{-1}. (b) Energy levels at the mesoscopic TiO$_2$/EMITFSI interface. Reprinted with permission from [12]. Copyright (2005) The American Chemical Society.

potential axis, Fig. 13. In this figure, the shift is approximately 450 mV, in good agreement with, the predicted 59 mV/pH unit. A similar shift is also observed in Fig. 12b; however, in this case the shift is accompanied by a change in the slope, which indicates a modification of the DOS.

A shift of the conduction band also occurs if instead of changing the concentration of protons in aqueous solution, the size or concentrations of cations added to a polar solution are modified, Fig. 14.
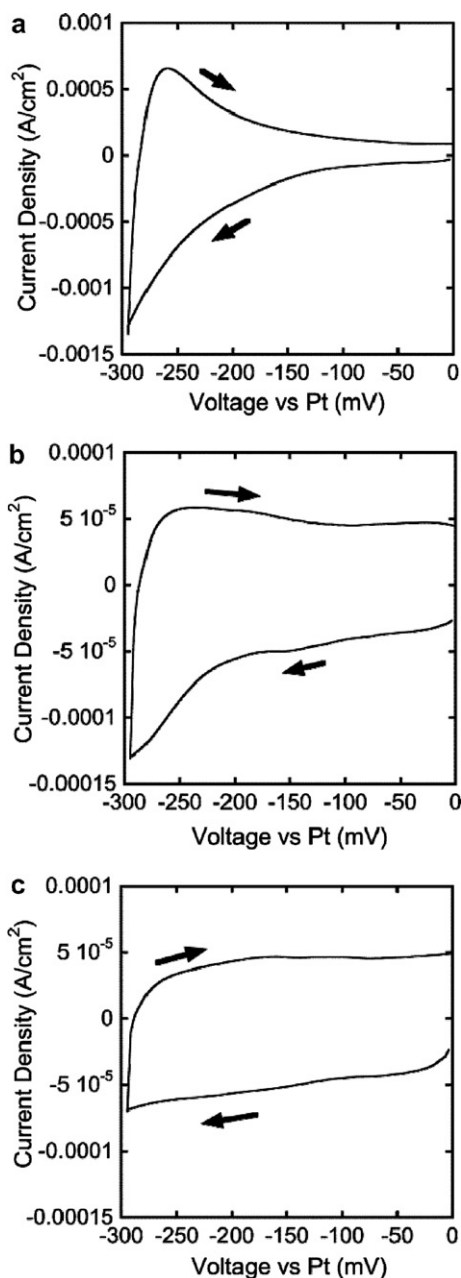
Fig. 15 shows the CVs for an 8 μm-thick layer of 20-nm-sized TiO$_2$ particles [12], first sensitized with an amphiphilic ruthenium sensitizer [Ru (4,4′-dicarboxylic acid-2,2′-bipyridine) (4,4′-bis(*p*-hexyloxystyryl)-2,2′-bipyridine)(NCS)2], coded as K-19, and then co-grafted 4-guanidinobutyric acid (GBA) as a coadsorbent. The electrolyte is the ionic liquid EMITFSI. The CVs reveal that the addition of GBA negatively shifts the conduction band of TiO$_2$. This shift produces an increase of photovoltage in a DSC, though this gain is usually accompanied by a decrease of photocurrent due to less efficient injection of photoexcited electrons. However, Grätzel and coworkers showed [12] that the bandshift by coadsorption GBA is small enough not to affect the electron injection from the excited sensitizer into the conduction band of TiO$_2$. Furthermore, GBA also inhibits recombination. These modifications cause the solar cell efficiency to increase by 0.6% at 1 sun.

Fig. 16 shows the CVs of nanoparticulate electrodes of different mixtures of ZnO and SnO$_2$ electrodes. In principle only the SnO$_2$ displays the exponential distribution, while the other electrodes show a constant capacitance, usually related to the exposed substrate area as discussed above. However, measurements of capacitance over a broader potential range, Fig. 17, show that in fact all the electrodes contain the exponential distribution, although at very different potentials.

As commented before, in solar cells and other devices with electron acceptor species in solution, the CV may not inform about DOS as it will be dominated by charge transfer reactions (resistances) that will hide the capacitive behavior. The effect of the accumulation of charge in TiO$_2$ is a slight hysteresis in the CV curve that is not always visible, see Fig. 18a. However, using IS it is possible to accurately determine the capacitance and thus the shift in the conduction band, Fig. 18b.
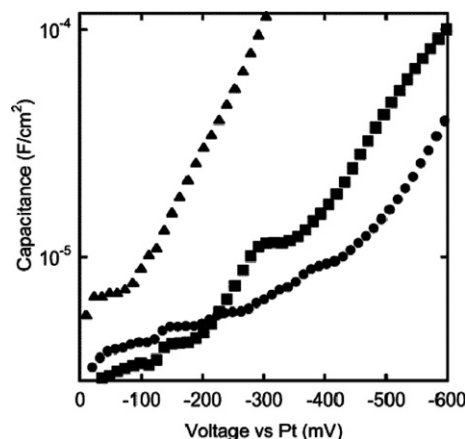

Fig. 16. Cyclic voltametries of (a) SnO$_2$, (b) ZnO, and (c) 53 wt% ZnO electrode under dark conditions at a scan rate of 10 V s^{-1}. The measurements were carried out on the DSCs fabricated with those electrodes. The arrows indicate scan directions. Reprinted with permission from [13]. Copyright (2005) The American Chemical Society.

Fig. 17. Estimated capacitances of SnO$_2$ (triangles), ZnO (squares), and 53 wt% ZnO (circles) electrodes obtained from CVs. The scan rates were 10 V s^{-1}. Reprinted from [13] with permission from The American Chemical Society.
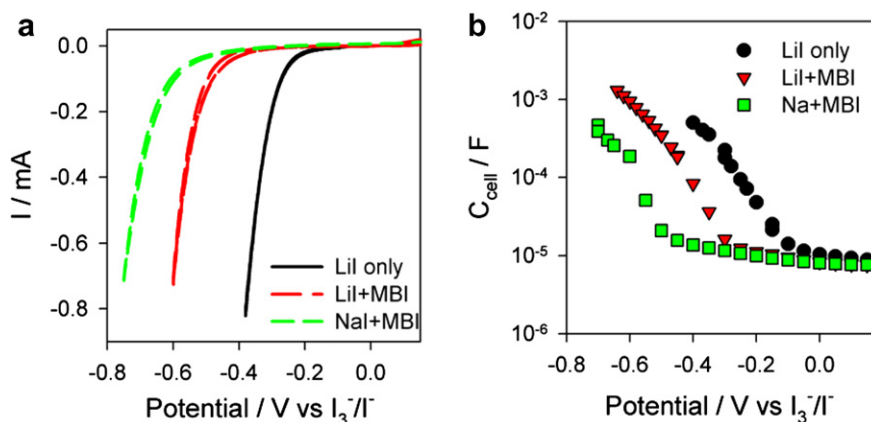
Fig. 18. Effect of changing electrolyte components in dye solar cell on the CV (a) and on the capacitance plot (b). Reprinted with permission from [74]. Copyright (2005) Elsevier.

Several groups have reported approaches to the deposition of electron recombination "blocking layers". As some examples, Tennakone et al. have recently reported the preparation of MgO coated TiO_2 for large area DSC [91]. Extensive work has been published on the use of metal oxide barriers [66,92,93] and it was observed that in spite of the fact that all the metal oxides conformaly deposited onto the surface of the nanoparticles show slow recombination dynamics, only those "blocking layers" made of Al_2O_3 or MgO oxides show weak improvement on recombination losses when compared with the bare nanoparticles. It was shown using electrochemical methods that this behavior can be rationalized in terms of the influence of the acid/base properties of the overlayer on the electron density of the TiO_2 [93]. The metal oxides overlayers of Al_2O_3 or MgO are more basic than TiO_2 and serve to raise the TiO_2 conduction band, therefore minimizing the increase in electron density and thereby the acceleration of the recombination dynamics under negative bias. Moreover, the analysis of the impedance data suggests that the metal oxide coatings also pasivate the surface trap states at the semiconductor nanoparticles [21,93], meaning that the only recombination pathway for the Al_2O_3 coated nanoparticles must be the electrons at the TiO_2 conduction band.

4.3. Molecular functionalization of nanoporous TiO_2

Functionalization of TiO_2 surface with donor/acceptor molecules is a key step for realizing devices and applications. The CV method is important for studying the redox properties of organic molecules attached in the TiO_2 surface, as in the case of viologen molecules [15] and proteins [16,17]. Provided that there is fast electron exchange between the semiconductor and the attached species, the functionalized electrode will show an excess of capacitance in the CV corresponding to the chemical (redox) capacitance of the molecular species, in comparison with the bare TiO_2 electrode.

In the following example, we consider a layer of viologen which is a cromophore, transparent in its neutral state

and dark blue in its first oxidized state (pale yellow after irreversible second oxidation), deposited on mesoporous TiO_2. The resulting voltammetry of the functionalized film, Fig. 19, consists on the addition of the characteristic voltammetry of TiO_2 shown in Fig. 6a and the response of the viologen molecules adsorbed on the surface.

Therefore, a good approximation of the characteristic voltammetry of the viologen attached to TiO_2, may be obtained by simple subtraction of TiO_2 response to the overall voltammetry of the film.

The quality of this approximation may be confirmed by simultaneous acquisition of absorbance data of the viologen activated films during the CV. From Beer–Lambert law the absorbance is

$$A = \varepsilon L c_{red} \qquad (11)$$

Here, ε is the molar absorption coefficient of reduced viologen, L the film thickness and c_{red} the concentration of reduced viologen molecules. Deriving this expression with respect to the potential, we obtain

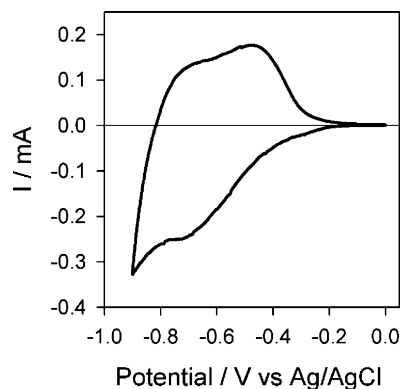$$\frac{dA}{dV} = \varepsilon L \frac{dc_{red}}{dV} \qquad (12)$$

Fig. 19. CV of a viologen-functionalized TiO_2 film. Reprinted with permission from [10]. Copyright (2004) Elsevier.
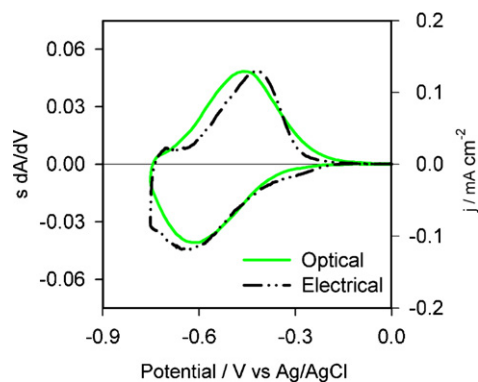
Fig. 20. The derivative of the absorbance of viologen attached to the surface of a nanoporous TiO$_2$ film with respect to the voltage, continuous line, and the voltammetry, dashed line, obtained by subtracting from the response of the whole film the bare TiO$_2$ voltammetry. Reprinted with permission from [10]. Copyright (2004) Elsevier.

This last expression is equivalent to Eq. (1). Taking into account that dc_{red}/dt is the current density, j, of electrons entering viologen molecules divided by the electron charge and the length of the film, Eq. (12) yields

$$s\frac{dA}{dV} = \frac{\varepsilon}{F}j \qquad (13)$$

where F is the Faraday constant. Fig. 20 shows that the electrical and optical methods give very similar results for the chemical capacitance of the viologen and thus it is possible to calculate the concentration of active molecules of viologen (i.e. the coverage) in the surface of the semiconductor. Alternatively, comparing the capacitance of the bare and functionalized TiO$_2$ we may compute the number of viologens and their energy distribution, Fig. 21.

The immobilization of redox actives biomolecules on mesoporous semiconductor films is currently attracting much interest for the development of biosensors and hydrogen evolving electrodes. A major contribution to the development of the area has been achieved using well-known proteins with haem groups such as hemoglobin [79,80] and cytochrome C [81]. Several groups have characterised the electrochemical properties of such protein/TiO$_2$

electrodes by cyclic voltammetry and demonstrated that the proteins can be fully reduced by the application of an electrical bias to the mesoporous film without the need of any electron-transfer mediators, Fig. 22. Note the similar patterns in Figs. 20 and 22 that display the addition of chemical capacitances of mesoporous TiO$_2$ and the surface molecular redox levels.
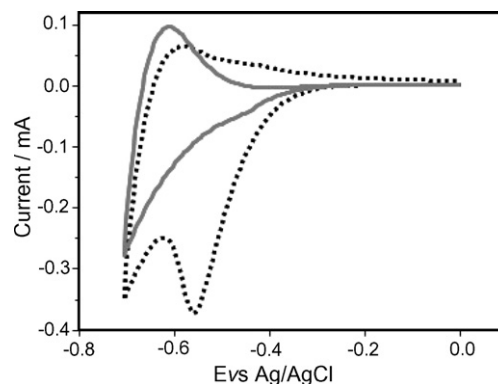

Fig. 22. Cyclic voltammetry of a 4 μm mesoporous TiO$_2$ film (grey) and the hemoglobin sensitised film (dots). Adapted from Ref. [79].
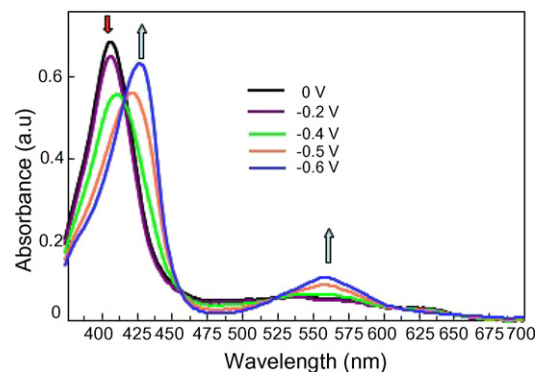

Fig. 23. Spectroelectrochemical data for the reduction of Hb/TiO$_2$ films upon increasing the negative potential from 0 V to −0.7 V vs. Ag/AgCl electrode. Adapted from Ref. [79].
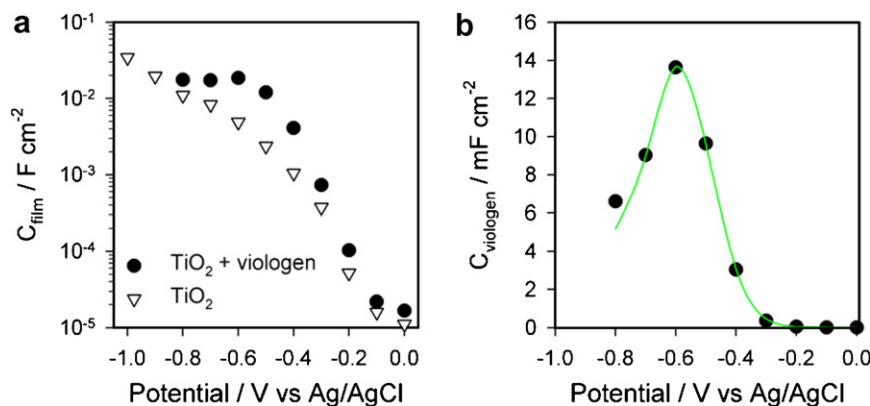

Fig. 21. (a) Capacitance of bare and viologen modified TiO$_2$. (b) Capacitance of viologen obtained from the difference between the previous ones. Distribution of DOS of viologen attached to the surface of titanium fits quite well to a Gaussian with a standard deviation of 63 mV.

The redox properties of the Hb/TiO_2 films can also be monitored using spectroelectrochemistry, since the reduction of the iron atom of the haem groups implies changes on the protein UV–Vis spectrum. Fig. 23 illustrates the changes on the absorption of Hb/TiO_2 from Fe^{III}–Hb to Fe^{II}–Hb. A clear shift in the Soret band from 406 to 428 nm can be observed as well as the formation of a new peak at 558 nm. The reversibility of the process has been utilized by Topoglidis et al. [79,81] to prepare a hybrid biosensor for nitric oxide (NO), which is a molecule involved in the chemical reactions that take place in the nervous system.

5. Results on organic conducting films

We will next show the type of analysis described above applied to two, commonly used, hole conducting materials, namely polypyrrole [9] and spiro-OMeTAD [10]. Some examples of CV response of electrochemically deposited polypyrrole films are shown in Fig. 24 for different substrates. In all cases CVs present similar characteristics: a rather broadened oxidation peak appears during the positive sweep at about 0.0 V versus Ag/AgCl for scan rates within the range 10–50 mV s^{-1}, followed by a current plateau at more positive potentials. For thin films and low scan rates, which are the usual experimental conditions that preclude kinetics limitations, the registered current is directly connected to the chemical capacitance of the polymer film, because the applied potential is close to that exerted on the charging process, as discussed in Section 3. The width at half-height of the oxidation peaks (~300 mV calculated from the anodic part of such peaks) is always quite high to be interpreted in terms of simple nernstian thermodynamics (90.6 mV or 181.2 mV depending upon the number of species involved). Moreover, the asymptotic response of the current as a function of the potential predicted by simple thermodynamics yields linear relationships of the form $\log j \propto (E - e\varepsilon)/nk_{B}T$, in which n corresponds to the number of species involved assuming

electroneutrality conditions. Fig. 25 shows CV response and fitting results using a Gaussian distribution of sites energies, Eq. (8). As observed in Fig. 25, excellent fit is obtained for the anodic part of the oxidation peak whilst the cathodic part is dominated by a current plateau. Hence, the shape of the oxidation peak is directly related to the shape of the electronic state distribution. Assuming that the holes, in available states corresponding to N molecules per unit volume, follow the zero-temperature Fermi distribution the overall result is that the chemical capacitance monitored by CV is proportional to the density-of-states as predicted from Eqs. (6) and (8). Values of $\sigma \approx 170$ meV and $N \approx 10^{21}$ cm^{-3} have been obtained from fits.

Fig. 26 shows the CV response of a 100-nm thick film comprised of spiro-OMeTAD molecules adsorbed onto ITO. The initial oxidation processes of the spiro-OMeTAD molecules appear to be better resolved. The first oxidation peak at ~0.55 V versus Ag/AgCl/KCl is the most important feature, taking into account that it is the potential at
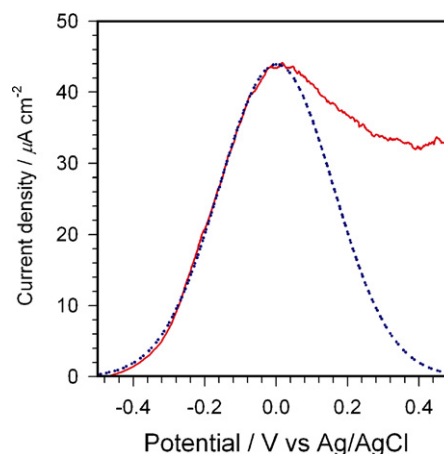

Fig. 25. Comparison between CV response for potentials near the oxidation peak of polypyrrole films onto ITO substrate and 60 mC cm^{-2} of polymerization charge (continuous) and fit (dotted) using a Gaussian distribution of states ($\sigma = 160$ meV, E_0 1.0 meV and $N = 1.8 \times 10^{21}$ cm^{-3}). Adapted from Ref. [9].
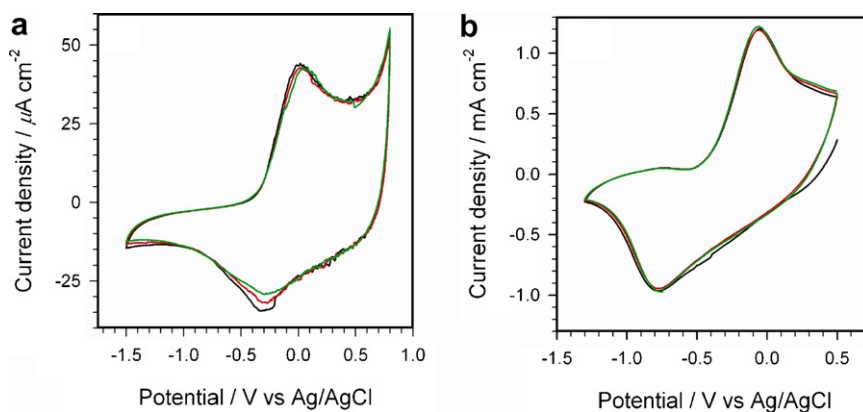

Fig. 24. Stable cyclic voltammograms of polypyrrole films in a solution of 0.1 M $LiClO_4$ in propylene carbonate. (a) Onto ITO substrate and 60 mC cm^{-2} of polymerization charge. Scan rate was 10 mV s^{-1}. (b) Onto Pt substrate and 120 mC cm^{-2} of polymerization charge. Scan rate was 50 mV s^{-1}. Adapted from Ref. [9].
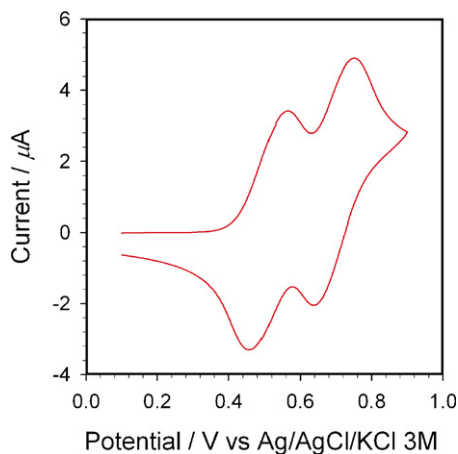
Fig. 26. Cyclic voltammetry of spiro-OMeTAD deposited onto ITO in a solution of 0.1 M KPF_6 in propylene carbonate. Scan rate was 10 mV s^{-1}. Reprinted from [10], Copyright (2006), with permission from Elsevier.
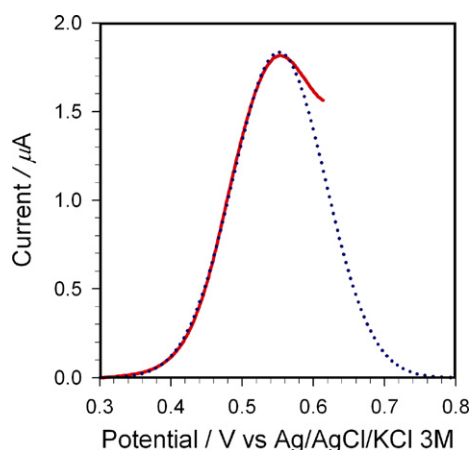

Fig. 27. Comparison between CV for the first oxidation peak of OMeTAD film onto ITO substrate (solid) and fit (dotted) using a Gaussian distribution of states ($\sigma = 65$ meV, $E_0 = 552$ meV and $N = 2.9 \times 10^{19}$ cm^{-3}). Reprinted from [10], Copyright (2006), with permission from Elsevier.

which the spiro-OMeTAD film switches from an insulating to a conducting state. The first oxidation peak of the CV exhibits a width at half height of ∼160 mV. As discussed above in the case of polypyrrole films, such value is unusually high when compared to the nernstian width for one-electron transfer. Again we interpret this result assuming that the oxidation energy levels are distributed according to a Gaussian expression given in Eq. (8). As observed in Fig. 27, an excellent fit is obtained for the anodic part of the oxidation peak. From this graph, values of 154 meV width at the half height of the peak ($\sigma = 65$ meV) and $N = 2.9 \times 10^{19}$ cm^{-3} are obtained.

Acknowledgements

References

[1] B. O' Regan, M. Grätzel, Nature 353 (1991) 737.
[2] A. Hagfeldt, M. Grätzel, Chem. Rev. 95 (1995) 49.
[3] M. Grätzel, Nature 414 (2001) 338.
[4] M. Grätzel, Nature 409 (2001) 575.
[5] S. Cosnier, A. Senillou, M. Grätzel, P. Comte, N. Vlachopoulos, N.J. Renault, C. Martelet, J. Electroanal. Chem. 469 (1999) 176.
[6] Q. Wang, S.M. Zakeeruddin, J. Cremer, P. Bäuerle, R. Humphry-Baker, M. Grätzel, J. Am. Chem. Soc. 127 (2005) 5706.
[7] F. Fabregat-Santiago, I. Mora-Seró, G. Garcia-Belmonte, J. Bisquert, J. Phys. Chem. B 107 (2003) 758.
[8] J. Bisquert, Phys. Chem. Chem. Phys. 5 (2003) 5360.
[9] J. Bisquert, G. Garcia-Belmonte, J. García-Cañadas, J. Chem. Phys. 120 (2004) 6726 .
[10] J. García-Cañadas, F. Fabregat-Santiago, H. Bolink, E. Palomares, G. Garcia-Belmonte, J. Bisquert, Synthetic Met. 156 (2006) 944.
[11] L. Kavan, K. Kratochvilova, M. Grätzel, J. Electroanal. Chem. 394 (1995) 93.
[12] Z. Zhang, S.M. Zakeeruddin, B.C. O'Regan, R. Humphry-Baker, M. Grätzel, J. Phys. Chem. B 109 (2005) 21818.
[13] D. Niinobe, Y. Makari, T. Kitamura, Y. Wada, S. Yanagida, J. Phys. Chem. B 109 (2005) 17892.
[14] H. Randriamahazaka, F. Fabregat-Santiago, A. Zaban, J. García-Cañadas, G. Garcia-Belmonte, J. Bisquert, Phys. Chem. Chem. Phys. 8 (2006) 1827.
[15] J. García-Cañadas, F. Fabregat-Santiago, J. Kapla, J. Bisquert, G. Garcia-Belmonte, I. Mora-Seró, M.O.M. Edwards, Electrochim. Acta 49 (2004) 745.
[16] Q. Li, G. Luo, J. Feng, Eletroanalysis 13 (2001) 359.
[17] E. Topoglidis, E. Palomares, Y. Astuti, A. Green, C.J. Campbell, J.R. Durrant, Electroanalysis 17 (2005) 1035.
[18] E.V. Milsom, H.A. Dash, A. Toby, A. Jenkins, M. Opallo, F. Marken, Bioelectrochemistry (2006).
[19] S. Tirosh, T. Dittrich, A. Ofir, L. Grinis, A. Zaban, J. Phys. Chem. B 110 (2006) 16165.
[20] G.K. Mor, O.K. Varghese, M. Paulose, K. Shankar, C.A. Grimes, Sol. Energy Mater. Sol. Cells 90 (2006) 2011.
[21] M. Law, L.E. Greene, A. Radenovic, T. Kuykendall, J. Liphardt, P. Yang, J. Phys. Chem. B 110 (2006) 22652.
[22] I. Mora-Seró, F. Fabregat-Santiago, B. Denier, J. Bisquert, R. Tena-Zaera, J. Elias, C. Lévy-Clement, Appl. Phys. Lett. 89 (2006) 203117.
[23] V.G. Kytin, J. Bisquert, I. Abayev, A. Zaban, Phys. Rev. B 70 (2004) 193304.
[24] J. Jamnik, J. Maier, Phys. Chem. Chem. Phys. 3 (2001) 1668.
[25] A. Zaban, O.I. Micic, B.A. Gregg, A.J. Nozik, Langmuir 14 (1998) 3153.
[26] R. Plass, S. Pelet, J. Krueger, M. Grätzel, J. Phys. Chem. B 106 (2002) 7578.
[27] I. Robel, V. Subramanian, M. Kuno, P.V. Kamat, J. Am. Chem. Soc. 128 (2006) 2385.
[28] R. Vogel, P. Hoyer, H. Weller, J. Phys. Chem. B 98 (1994) 3183.
[29] R.J. Ellingson, M.C. Beard, J.C. Johnson, P. Yu, O.I. Micic, A.J. Nozik, A. Shabaev, A.L. Efros, Nano Lett. 5 (2005) 865.
[30] R.D. Schaller, V.I. Klimov, Phys. Rev. Lett. 92 (2004) 186601.
[31] R.D. Schaller, M. Sykora, J.M. Pietryga, V.I. Klimov, Nano Lett. 6 (2006) 424.
[32] D. Vanmaekelbergh, P. Liljerorth, Chem. Soc. Rev. 34 (2005) 299.
[33] D. Yu, C. Wang, P. Guyot-Sionnest, Science 300 (2003) 1277.
[34] A.J. Houtepen, D. Vanmaekelbergh, J. Phys. Chem. B 109 (2005) 19634.
[35] A.L. Roest, A.J. Houtepen, J.J. Kelly, D. Vanmaekelbergh, Faraday Discuss 125 (2004) 55.
[36] A.L. Roest, J.J. Kelly, D. Vanmaekelbergh, Appl. Phys. Lett. 83 (2003) 5530.
[37] N. Kopidakis, N.R. Neale, K. Zhu, J. van de Lagemaat, A.J. Frank, Appl. Phys. Lett. 87 (2005) 202106.

[38] B.E. Conway, Electrochemical Supercapacitors, Plenum Publishing, New York, 1999.

[39] C.E.D. Chidsey, R.W. Murray, J. Phys. Chem. 90 (1986) 1479.

[40] R.A. Marcus, Rev. Mod. Phys. 65 (1993) 599.

[41] H. Gerischer, Electrochim. Acta 35 (1990) 1677.

[42] J. Bisquert, A. Zaban, P. Salvador, J. Phys. Chem. B 106 (2002) 8774.

[43] J. Bisquert, A. Zaban, M. Greenshtein, I. Mora-Seró, J. Am. Chem. Soc. 126 (2004) 13550.

[44] S.R. Morrison, Electrochemistry at Semiconductor and Oxidized Metal Electrodes, Plenum Press, New York, 1980.

[45] A.M. Becka, C.J. Miller, J. Phys. Chem. 96 (1992).

[46] J. Bisquert, E. Palomares, C.A. Quiñones, J. Phys. Chem. B 110 (2006) 11284.

[47] U. Bach, D. Lupo, P. Comte, J.E. Moser, F. Weissörtel, J. Salbeck, H. Spreitzer, M. Grätzel, Nature 398 (1998) 583.

[48] J. Krüger, R. Plass, L. Cevey, M. Piccirelli, M. Grätzel, U. Bach, Appl. Phys. Lett. 79 (2001) 2085.

[49] J. Krüger, R. Plass, M. Grätzel, H.-J. Matthieu, Appl. Phys. Lett. 81 (2002) 367.

[50] H. Bässler, Phys. Stat. Sol. (b) 175 (1993) 15.

[51] I.N. Hulea, H.B. Brom, A.J. Houtepen, D. Vanmaekelbergh, J.J. Kelly, E.A. Meulenkamp, Phys. Rev. Lett. 93 (2004) 166601.

[52] C. Tanase, P.W.M. Blom, D.M. de Leeuw, E.J. Meijer, Phys. Stat. Sol. (a) 201 (2004) 1236.

[53] A. Dieckmann, H. Bässler, P.M. Borsenberg, J. Chem. Phys. 99 (1993) 8136.

[54] Z.G. Yu, D.L. Smith, A. Saxena, R.L. Martin, A.R. Bishop, Phys. Rev. B 63 (2001) 085202.

[55] R. Richert, L. Pautmeier, H. Bässler, Phys. Rev. Lett. 63 (1989) 547.

[56] R. Coehoorn, W.F. Pasveer, P.A. Bobbert, C.J. Michels, Phys. Rev. B 72 (2005) 155206.

[57] G. Garcia-Belmonte, V.S. Vikhrenko, J. García-Cañadas, J. Bisquert, Solid State Ionics 170 (2004) 123.

[58] J. Garcia-Cañadas, G. Garcia-Belmonte, J. Bisquert, I. Porqueras, C. Person, Solid State Ionics 176 (2005) 1701.

[59] G. Garcia-Belmonte, J. García-Cañadas, J. Bisquert, J. Phys. Chem. B 110 (2006) 4514.

[60] F. Fabregat-Santiago, J. Bisquert, G. Garcia-Belmonte, G. Boschloo, A. Hagfeldt, Sol. Energy Mater. Sol. Cells 87 (2005) 117.

[61] N.W. Duffy, L.M. Peter, R.M.G. Rajapakse, K.G.U. Wijayantha, Electrochem. Commun. 2 (2000) 658.

[62] L.M. Peter, N.W. Duffy, R.L. Wang, K.G.U. Wijayantha, J. Electroanal. Chem. 524–525 (2002) 127.

[63] G. Boschloo, L. Haggman, A. Hagfeldt, J. Phys. Chem. B 110 (2006) 13144.

[64] L.M. Peter, J. Electroanal. Chem. 599 (2007) 233.

[65] M. Bailes, P.J. Cameron, K. Lobato, L.M. Peter, J. Phys. Chem. B 109 (2005) 15429.

[66] E. Palomares, J.N. Clifford, S.A. Haque, T. Lutz, J.R. Durrant, J. Am. Chem. Soc. 125 (2003) 475.

[67] H.G. Agrell, G. Boschloo, A. Hagfeldt, J. Phys. Chem. B 108 (2004) 12388.

[68] I. Abayev, A. Zaban, V.G. Kytin, A.A. Danilin, G. Garcia-Belmonte, J. Bisquert, J. Solid State Electrochem. 11 (2007) 647.

[69] J. Bisquert, A. Zaban, Appl. Phys. A 77 (2003) 507.

[70] A. Hauch, A. Georg, Electrochim. Acta 46 (2001) 3457.

[71] J. Bisquert, J. Phys. Chem. B 106 (2002) 325.

[72] R. Kern, R. Sastrawan, J. Ferber, R. Stangl, J. Luther, Electrochim. Acta 47 (2002) 4213.

[73] F. Fabregat-Santiago, G. Garcia-Belmonte, J. Bisquert, A. Zaban, P. Salvador, J. Phys. Chem. B 106 (2002) 334.

[74] F. Fabregat-Santiago, J. Bisquert, G. Garcia-Belmonte, G. Boschloo, A. Hagfeldt, Solar Energy Mater. Solar Cells 87 (2005) 117.

[75] Q. Wang, J.E. Moser, M. Grätzel, J. Phys. Chem. B 109 (2005) 14945.

[76] T. Hoshikawa, R. Kikuchi, K. Eguchi, J. Electroanal. Chem. 588 (2006) 59.

[77] M. Adachi, M. Sakamoto, J. Jiu, Y. Ogata, S. Isoda, J. Phys. Chem. B 110 (2006) 13872.

[78] I. Abayev, A. Zaban, F. Fabregat-Santiago, J. Bisquert, Phys. Stat. Sol. (a) 196 (2003) R4.

[79] Q. Wang, S. Ito, M. Grätzel, F. Fabregat-Santiago, I. Mora-Seró, J. Bisquert, T. Bosshoa, H. Imaic, J. Phys. Chem. B 110 (2006) 19406.

[80] S. Ruhle, M. Greenshtein, S.-G. Chen, A. Merson, H. Pizem, C.S. Sukenik, D. Cahen, A. Zaban, J. Phys. Chem. B 109 (2005) 18907.

[81] F. Fabregat-Santiago, G. Garcia-Belmonte, J. Bisquert, P. Bogdanoff, A. Zaban, J. Electrochem. Soc. 150 (2002) E293.

[82] T. Berger, T. Lana Villarreal, D. Monllor-Satoca, R. Gómez, J. Phys. Chem. C (2007) doi:10.1021/jp071438p.

[83] K. Zhu, N. Kopidakis, N.R. Neale, J. van de Lagemaat, A.J. Frank, J. Phys. Chem. B 110 (2006) 25174.

[84] J.I. Pankove, Optical Processes in Semiconductors, Prentice-Hall, Englewood Cliffs, NJ, 1971.

[85] T. Dittrich, I. Mora-Seró, G. Garcia-Belmonte, J. Bisquert, Phys. Rev. B 73 (2006) 045407.

[86] I. Mora-Seró, J.A. Anta, G. Garcia-Belmonte, T. Dittrich, J. Bisquert, J. Photochem. Photobiol. A: Chem. 182 (2006) 280.

[87] J.L. Movilla, G. Garcia-Belmonte, J. Bisquert, J. Planelles, Phys. Rev. B 72 (2005) 153313.

[88] W.H. Leng, Z. Zhang, Z.Q. Zhang, C.N. Cao, J. Phys. Chem. B 109 (2005) 15008.

[89] G. Boschloo, D. Fitzmaurice, J. Phys. Chem. B 103 (1999) 2228.

[90] H. Wang, J. He, G. Boschloo, H. Lindström, A. Hagfeldt, S. Lindquist, J. Phys. Chem. B 105 (2001) 2529.

[91] G.R.A. Kumara, S. Kaneko, A. Konno, M. Okuya, T.N. Murakami, B. Onwona-Agyeman, K. Tennakone, Prog. Photov.: Res. Appl. 14 (2006) 643.

[92] Y. Diamant, S.G. Chen, O. Melamed, A. Zaban, J. Phys. Chem. B 107 (2003) 1977.

[93] F. Fabregat-Santiago, J. García-Cañadas, E. Palomares, J.N. Clifford, S.A. Haque, J.R. Durrant, G. Garcia-Belmonte, J. Bisquert, J. Appl. Phys. 96 (2004) 6903.